Systemic low-dose erythropoietin administration improves the vascularization of collagen-glycosaminoglycan matrices seeded with adipose tissue-derived microvascular fragments

Thomas Später[1] iD, **Denise MS Worringer**[1], **Maximilian M Menger**[1,2], **Michael D Menger**[1] and **Matthias W Laschke**[1] iD

Abstract

Adipose tissue-derived microvascular fragments (MVF) are used as vascularization units in tissue engineering. In this study, we investigated whether the vascularization capacity of MVF can be improved by systemic low-dose erythropoietin (EPO) administration. MVF were isolated from the epididymal fat of donor mice and seeded onto collagen-glycosaminoglycan matrices, which were implanted into full-thickness skin defects within dorsal skinfold chambers of recipient mice. Both donor and recipient mice were treated daily with either EPO (500 IU/kg) or vehicle (0.9% NaCl). The implants were analyzed by stereomicroscopy, intravital fluorescence microscopy, histology, and immunohistochemistry. EPO-treated MVF contained a comparable number of proliferating Ki67$^+$ but less apoptotic cleaved caspase-3$^+$ endothelial cells when compared to vehicle-treated controls. Moreover, EPO treatment accelerated and improved the in vivo vascularization, blood vessel maturation, and epithelialization of MVF-seeded matrices. These findings indicate that systemic low-dose EPO treatment is suitable to enhance the viability and network-forming capacity of MVF.

Introduction

In clinical practice, autologous split-thickness skin grafts (STSG) represent the gold standard for the treatment of extensive full-thickness skin defects.[1,2] For the initial coverage of these defects, bioengineered substitutes, such as collagen-glycosaminoglycan (CGAG) matrices, are used to fulfil the functions of the cutaneous dermal layer and to stimulate both cellular infiltration and vascular ingrowth from the surrounding host tissue in order to prepare the wound bed for a later STSG.[3,4] Noteworthy, the development of a sufficient vascularization within these matrices may require a relatively long time period of up to 3 weeks.[5]

Experimental studies indicate that dermal substitutes may be seeded with stem cells, keratinocytes or adipose tissue-derived microvascular fragments (MVF) to accelerate and improve their vascularization.[6–8] MVF represent fully functional microvessel segments, which can be easily isolated from fat samples by means of mechanical and enzymatical digestion.[9] After their seeding onto matrices, MVF have been shown to rapidly reassemble into new microvascular networks and to connect

[1]Institute for Clinical & Experimental Surgery, Saarland University, Homburg/Saar, Germany
[2]Department of Trauma and Reconstructive Surgery, Eberhard Karls University Tuebingen, BG Trauma Center Tuebingen, Tuebingen, Germany

Corresponding author:
Thomas Später, Institute for Clinical & Experimental Surgery, Saarland University, Kirrberger Staße; Geb. 65/66, Homburg/Saar 66421, Germany.
Email: thomas.spaeter@uks.eu

to the blood vessels of the surrounding host tissue. This, in turn, markedly improves the incorporation of the implants at the defect site.[10]

Of interest, we have recently demonstrated that a 24-h precultivation of isolated MVF in medium supplemented with erythropoietin (EPO) further improves their proliferation and in vivo vascularization capacity.[11] EPO is the main hematopoietic regulator of cellular proliferation and differentiation along the erythroid lineage and, thus, commonly used for the treatment of anemia.[12–18] The glycoprotein is released from the kidney in response to hypoxia and exerts its effects by means of a conformational change of the erythropoietin receptor (EPOR).[19,20] Besides the stimulation of hematopoiesis, these effects include nitric oxide-mediated endothelium-dependent relaxation of arterial vessels,[21] prevention of apoptotic cell death,[22] and tissue regeneration.[23] Moreover, EPO is a strong promoter of angiogenesis.[24] Numerous studies could demonstrate that EPO treatment results in the formation of angiogenic sprouts originating from pre-existing blood vessels.[25,26] This sprout formation also represents a crucial step in both the reassembly of individual MVF to new microvascular networks and their interconnection with the microvasculature of the surrounding tissue.[27]

In an ideal clinical setting, MVF may be rapidly isolated from liposuctioned fat and directly retransferred into a tissue defect of the patient within an intra-operative one-step procedure. Accordingly, the angiogenic stimulation of MVF by EPO during a 24-h precultivation phase may not be expedient. Alternatively, their vascularization capacity may be improved by systemic EPO treatment of the patient. To test this hypothesis, we herein isolated MVF from the epididymal fat pads of vehicle- and EPO-treated donor mice. The MVF were then seeded onto CGAG matrices, which were subsequently implanted into full-thickness skin defects within dorsal skinfold chambers of vehicle- and EPO-treated recipient animals. The vascularization and incorporation of the implanted matrices were analyzed by means of intravital fluorescence microscopy, histology and immunohistochemistry throughout an observation period of 2 weeks.

Materials and methods

Animals

Dorsal skinfold chambers were implanted in C57BL/6 wild-type mice (Institute for Clinical & Experimental Surgery, Saarland University, Homburg, Germany) with an age of 3–6 months and a body weight of 24–28 g. Epididymal fat was isolated from green fluorescent protein (GFP)+ mice (C57BL/6-Tg(CAG-EGFP)1Osb/J; The Jackson Laboratory, Bar Harbor, ME, USA) with an age of 7–12 months and a body weight of >30 g. The animals were housed under a 12 h day/night cycle and received water and standard pellet food (Altromin, Lage, Germany) ad libitum.

Isolation of MVF

As previously described in detail, MVF (Figure 1(a)) were isolated from the epididymal fat pads of GFP+ C57BL/6 donor mice.[8,9] For this purpose, the animals were anesthetized by an intraperitoneal (i.p.) injection of ketamine (75 mg/kg body weight; Ursotamin®; Serumwerke Bernburg, Bernburg, Germany) and xylazine (25 mg/kg body weight; Rompun®; Bayer, Leverkusen, Germany). The harvested adipose tissue was transferred into 10% Dulbecco's modified eagle medium (DMEM; 100 U/mL penicillin, 0.1 mg/mL streptomycin; Biochrom, Berlin, Germany) and washed thrice with phosphate-buffered saline (PBS). Subsequently, collagenase NB4G (0.5 U/mL; Serva Heidelberg, Germany) was used to enzymatically digest the fat tissue under slight stirring and humidified atmospheric conditions (37°C, 5% CO_2) for ~10 min. Thereafter, two volumes of PBS supplemented with 20% fetal calf serum (FCS) were used to neutralize the enzymatic digestion. After incubation of the cell-vessel suspension for 5 min at 37°C, the supernatant was removed and the resulting suspension was filtered through a 500 μm mesh. Subsequently, MVF were enriched to a pellet by a 5-min centrifugation at 120*g*. Finally, the remaining MVF pellet was resuspended in 10 μL of 0.9% NaCl for the seeding of CGAG matrices.

Seeding of CGAG matrices

A 4-mm biopsy punch (kaiEurope GmbH, Solingen, Germany) was used to cut identical 12.5 mm² samples out of a 1.3 mm-thick Integra® Dermal Regeneration Template Single Layer without silicone sheet (Integra Life Sciences, Ratingen, Germany). The matrices were then placed on a 500 μm cell strainer and 10 μL 0.9% NaCl containing ~20,000 MVF and ~200,000 single cells were transferred onto the matrices with a 20 μL pipette (Eppendorf, Wesseling-Berzdorf, Germany) (Figure 1(b)). This pipette was additionally used to induce negative pressure from underneath the CGAG matrices to ensure a sufficient seeding depth of MVF.[10] The MVF-seeded matrices were then either directly processed for further histological and immunohistochemical analyses or implanted into full-thickness skin defects for in vivo analyses.

Modified dorsal skinfold chamber model

MVF-seeded CGAG matrices were implanted into full-thickness skin defects within dorsal skinfold chambers of GFP- C57BL/6 recipient mice. This approach offers the main advantage to provide continuous access for repetitive in vivo analyses of wound defects.[28] Prior to the implantation of the dorsal skinfold chamber (Irola Industriekomponenten GmbH & Co. KG, Schonach, Germany), the mice were anesthetized by an i.p. injection of ketamine (75 mg/kg body weight; Ursotamin®) and xylazine (25 mg/kg body weight; Rompun®). For pain
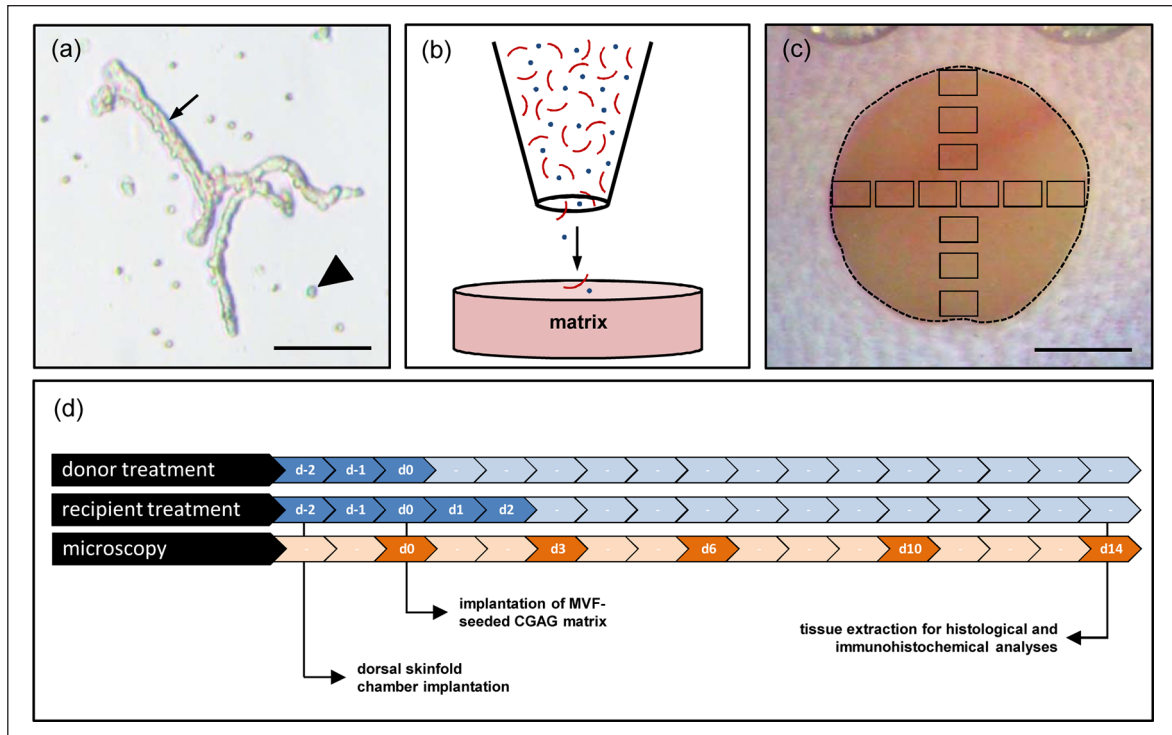
Figure 1. Experimental setting of the study: (a) freshly isolated MVF (arrow) with surrounding single cells (arrowhead) from the epididymal fat pads of a GFP[+] donor mouse. Scale bar: 65 μm, (b) schematic illustration of CGAG matrix seeding with MVF (red) and single cells (blue), (c) overview of the chamber observation window directly after implantation of a CGAG matrix (broken line = matrix border; black frames = ROIs for intravital fluorescence microscopy). Scale bar: 1.6 mm, and (d) schematic overview of the experimental protocol of the present study. To mimic an autologous transplantation of MVF, as envisaged for their future clinical application, both donor and recipient mice of MVF were treated with EPO or vehicle (control) on day −2, −1, and 0. The treatment of the recipient mice was continued on day 1 and 2. Dorsal skinfold chambers were prepared in the recipient mice on day −2 followed by the implantation of MVF-seeded CGAG matrices on day 0. Microscopic analyses of the implants were performed on day 0, 3, 6, 10, and 14. Thereafter, the implants were excised for further histological and immunohistochemical analyses.

medication, all animals received a subcutaneous (s.c.) injection of 5 mg/kg Carprofen (Rimadyl®; Zoetis Deutschland GmbH, Berlin, Germany) at the beginning of the surgical procedure. Thereafter, the two symmetrical titanium frames of the chamber were fixed on the extended dorsal skinfold of the animals, as previously described in detail.[29] After the mice were allowed to recover for 48 h, a 4-mm full-thickness skin defect was created within the observation window of the chamber by means of a dermal biopsy punch (kaiEurope GmbH). Immediately after wound creation, the defect was filled with a MVF-seeded CGAG matrix and the observation window was sealed with a removable cover glass.

Stereomicroscopy

To analyze both the epithelialization and hemorrhage formation of implanted CGAG matrices by means of planimetry, the anesthetized mice were fixed on a plexiglas stage and the dorsal skinfold chamber was positioned under a stereomicroscope (Leica M651, Wetzlar, Germany) on day 0 (day of implantation), 3, 6, 10, and 14. Then, the chamber tissue was visualized in epi-illumination to detect epithelialized and non-epithelialized implant areas. The epithelialized area (given in %) was calculated by the equation: (total implant area − non-epithelialized implant area)/(total implant area) × 100. Subsequently, the extent of bleeding (given in % of implant surface) induced by the MVF-seeded matrices was detected by means of trans-illumination microscopy. Bleeding was evaluated with the use of a semiquantitative score, which is defined as follows: 1: no bleeding, 2: 1%–25%, 3: 26%–50%, 4: 51%–75%, 5: 76%–100%, 6: bleeding exceeding the implant surface. All microscopic images were recorded on DVD and subsequently analyzed using the computer-assisted off-line analysis system CapImage (Zeintl, Heidelberg, Germany).

Intravital fluorescence microscopy

Following the stereomicroscopic analyses of the CGAG matrices, the anesthetized mice were retrobulbarily injected with 0.1 mL of the blood plasma marker 5% fluorescein isothiocyanate (FITC)-labeled dextran (150,000 Da; Sigma-Aldrich, Taufkirchen, Germany) for contrast enhancement.

Subsequently, the chamber window was placed under a Zeiss Axiotech fluorescence epi-illumination microscope (Zeiss, Oberkochen, Germany). The microscopic images were recorded with a charge-coupled device video camera (FK6990; Pieper, Schwerte, Germany) and a DVD system for off-line analyses using CapImage (Zeintl). The vascularization of the implanted matrices was assessed in 12 regions of interest (ROIs) (Figure 1(c)). ROIs exhibiting red blood cell (RBC)-perfused microvessels were defined and counted as perfused ROIs (% of all ROIs). Furthermore, the total length of all RBC-perfused blood vessels was measured to calculate the functional microvessel density per ROI (cm/cm^2). Additionally, both diameter (d, μm) and centerline RBC velocity (v, μm/s) of 40 randomly selected microvessels within the implants were measured. These two parameters were then used to calculate the wall shear rate (y, s^{-1}) by means of the Newtonian definition y = 8 × v/d.

Histology and immunohistochemistry

Formalin-fixed specimens of freshly MVF-seeded CGAG matrices as well as dorsal skinfold preparations containing MVF-seeded CGAG matrices were embedded in paraffin and cut into 3 μm-thick sections. Hematoxylin and eosin (HE) staining was first performed on individual sections of all samples according to standard procedures. To quantify the collagen content of implanted MVF-seeded matrices after 14 days, additional sections were stained with Sirius red. Using a BX60 microscope (Olympus, Hamburg, Germany) and the imaging software cellSens Dimension 1.11 (Olympus), the collagen content in relation to that of normal skin was assessed in four ROIs of each sample.[8]

Moreover, dorsal skinfold preparations were co-stained with a monoclonal rat anti-mouse antibody against the endothelial cell marker CD31 (1:100; Dianova, Hamburg, Germany) and a polyclonal goat antibody against GFP (1:200; Rockland Immunochemicals, Limerick, PA, USA) followed by a goat anti-rat IgG Alexa555 antibody (Life Technologies, Ober-Olm, Germany) and a biotinylated donkey anti-goat antibody (1:30; Dianova) as secondary antibodies. The biotinylated antibody was detected by streptavidin-Alexa 488 (1:50; Life Technologies) and cell nuclei were stained with Hoechst 33342 (2 μg/mL; Sigma-Aldrich). Quantitative analyses of these sections included the determination of the density of CD31$^+$ microvessels (given in mm^{-2}) and the fraction of CD31$^+$/GFP$^+$ microvessels (given in %) within the matrices.

For the detection of Ki67$^+$ and cleaved caspase-3 (CC3)$^+$ endothelial cells, sections of freshly seeded MVF-containing matrices were co-stained with a monoclonal rat anti-mouse antibody against the endothelial cell marker CD31 (1:100; Dianova) and a rabbit polyclonal anti-Ki67 antibody (1:500; Abcam, Cambridge, UK) or a rabbit polyclonal anti-CC3 antibody (1:100; New England Biolabs, Frankfurt, Germany) as primary antibodies followed by a goat anti-rat IgG Alexa555 antibody (Life Technologies) and a biotinylated goat anti-rabbit IgG antibody (ready-to-use; Abcam) as secondary antibodies. The biotinylated antibody was detected by peroxidase-labeled-streptavidin (1:50; Sigma-Aldrich). 3-Amino-9-ethylcarbazole (Abcam) was used as chromogen. Quantitative analyses of these sections included the determination of the fractions of Ki67$^+$ and CC3$^+$ endothelial cells (given in %) in six randomly selected ROIs within the freshly seeded matrices.

Experimental protocol

For in vitro and in vivo analyses, 12 GFP$^+$ donor mice were either pre-treated with EPO (n = 6; 500 IU/kg i.p. dissolved in 100 μL 0.9% NaCl; Roche Pharma, Basel, Switzerland) or vehicle (n = 6; 100 μL 0.9% NaCl) once daily for 3 days (Figure 1(d)). After the treatment period, GFP$^+$ MVF were isolated and seeded onto CGAG matrices (n = 22), as described above. Directly after seeding, six matrices were processed for the histological analysis of proliferating and apoptotic endothelial cells of the MVF. The remaining 16 matrices were implanted into full-thickness skin defects within dorsal skinfold chambers of 16 GFP$^-$ C57BL/6 wild-type mice. These recipient mice were treated with EPO (n = 8) or vehicle (n = 8) once daily for 5 days from the day of skinfold chamber implantation (day −2) (Figure 1(d)). By applying this treatment regimen, we mimicked an autologous transplantation of MVF, as envisaged for their future clinical application.

The hemorrhage formation, vascularization, epithelialization, and incorporation of the implants were assessed by means of repetitive stereomicroscopy and intravital fluorescence microscopy on day 0, 3, 6, 10, and 14. At the end of the 2-week observation period, all animals were sacrificed with an overdose of anesthesia and the dorsal skinfold chamber preparations were processed for histological and immunohistochemical analyses.

Statistical analysis

After testing the data for normal distribution and equal variance, differences between the groups were analyzed by the unpaired Student's *t*-test (SigmaPlot 11.0; Jandel Corporation, San Rafael, CA, USA). In case of non-parametric data, a Mann-Whitney rank sum test was used. All values are expressed as means ± SEM. Statistical significance was accepted for a value of *p* < 0.05.

Results

Proliferating and apoptotic endothelial cells of freshly isolated MVF

In a first set of experiments, we analyzed CGAG matrices directly after their seeding with EPO- and vehicle-treated MVF. Immunofluorescent microscopy of the
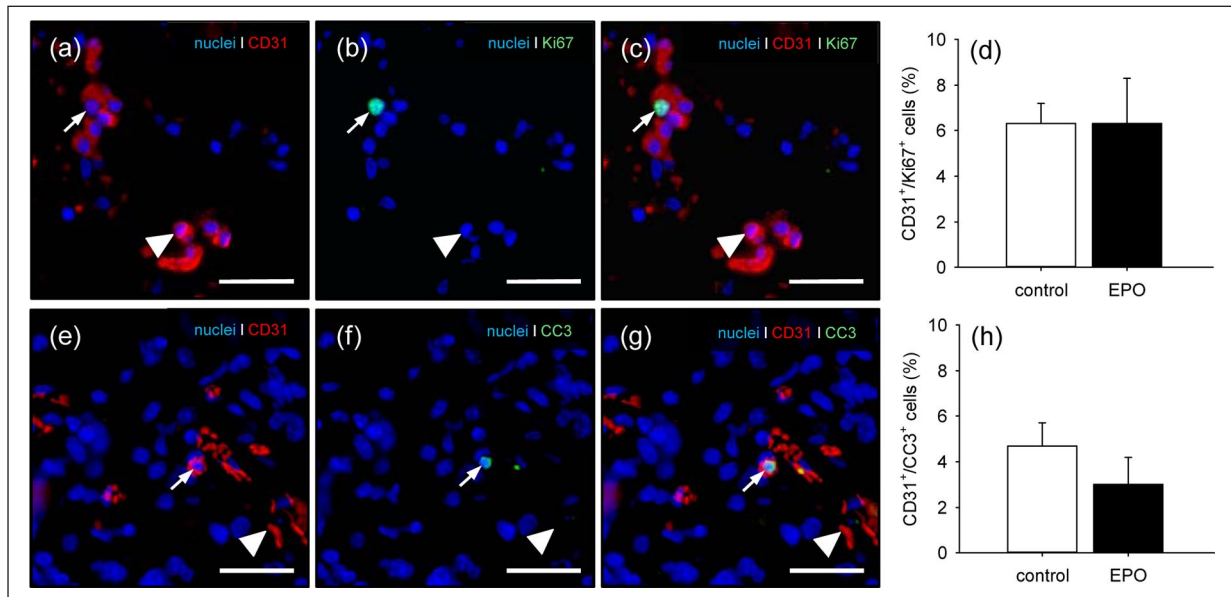
Figure 2. Proliferating and apoptotic endothelial cells in MVF: (a–c) representative images of the immunohistochemical detection of CD31$^+$/Ki67$^+$ (arrows) and CD31$^+$/Ki67$^-$ endothelial cells (arrowheads) of EPO-treated MVF within a CGAG matrix directly after seeding. Scale bars: 45 µm. (d) CD31$^+$/Ki67$^+$ endothelial cells (%) of vehicle- (control; white bar; $n = 3$) and EPO-treated (black bar; $n = 3$) MVF within CGAG matrices directly after seeding, as assessed by immunohistochemical analysis. Means ± SEM. (e–g) representative images of the immunohistochemical detection of CD31$^+$/CC3$^+$ (arrows) and CD31$^+$/CC3$^-$ endothelial cells (arrowheads) of EPO-treated MVF within a CGAG matrix directly after seeding. Scale bars: 45 µm, and (h) CD31$^+$/CC3$^+$ endothelial cells (%) of vehicle- (control; white bar; $n = 3$) and EPO-treated (black bar; $n = 3$) MVF within CGAG matrices directly after seeding, as assessed by immunohistochemical analysis. Means ± SEM.

samples showed a comparable fraction of proliferating Ki67$^+$ endothelial cells within the two groups (Figure 2(a)–(d)). In contrast, although not proven to be significant, EPO-treated MVF contained less apoptotic CC3$^+$ endothelial cells when compared to vehicle-treated controls (Figure 2(e)–(h)).

Vascularization of MVF-seeded matrices

The vascularization of CGAG matrices seeded with EPO- and vehicle-treated MVF was repetitively analyzed in the mouse dorsal skinfold chamber model by means of intravital fluorescence microscopy (Figure 3(a)–(f)). This analysis revealed a significantly higher number of perfused ROIs in the EPO group when compared to vehicle-treated controls on both days 6 and 10 (Figure 3(g)). This indicates an accelerated vascularization of matrices seeded with EPO-treated MVF. In addition, these matrices also exhibited a significantly higher functional microvessel density on both days 10 and 14 when compared to controls (Figure 3(h)).

During the phase of in vivo implantation, the newly developing microvascular networks within matrices seeded with EPO- and vehicle-treated MVF underwent a progressive maturation, as indicated by decreasing diameters as well as increasing centerline RBC velocities and wall shear rates of individual microvessels over time (Table 1). Of interest, this maturation process was more pronounced in

matrices seeded with EPO-treated MVF, which finally contained blood vessels with a smaller diameter and a higher wall shear rate when compared to controls (Table 1).

Implant-induced bleeding

All implants were additionally analyzed by means of transillumination stereomicroscopy to determine whether EPO-treatment promotes the formation of hemorrhages in MVF-seeded CGAG matrices. The highest hemorrhagic score for both groups was detected on day 6 after implantation (Figure 4(a)–(g)). Of interest, this score was significantly higher in the EPO group when compared to the control group. As already shown by intravital fluorescence microscopy, the newly developing microvascular networks were still incomplete and unorganized at this early phase of the vascularization process (Figure 3(b) and (e)). In the following time course of the experiment, the hemorrhages within all matrices were progressively resorbed, resulting in a final hemorrhagic score comparable to that directly after matrix implantation (Figure 4(g)).

Implant incorporation and vascularization

The matrices of both groups were additionally evaluated by means of histology and immunohistochemistry on day 14 after implantation. The analysis of HE-stained sections
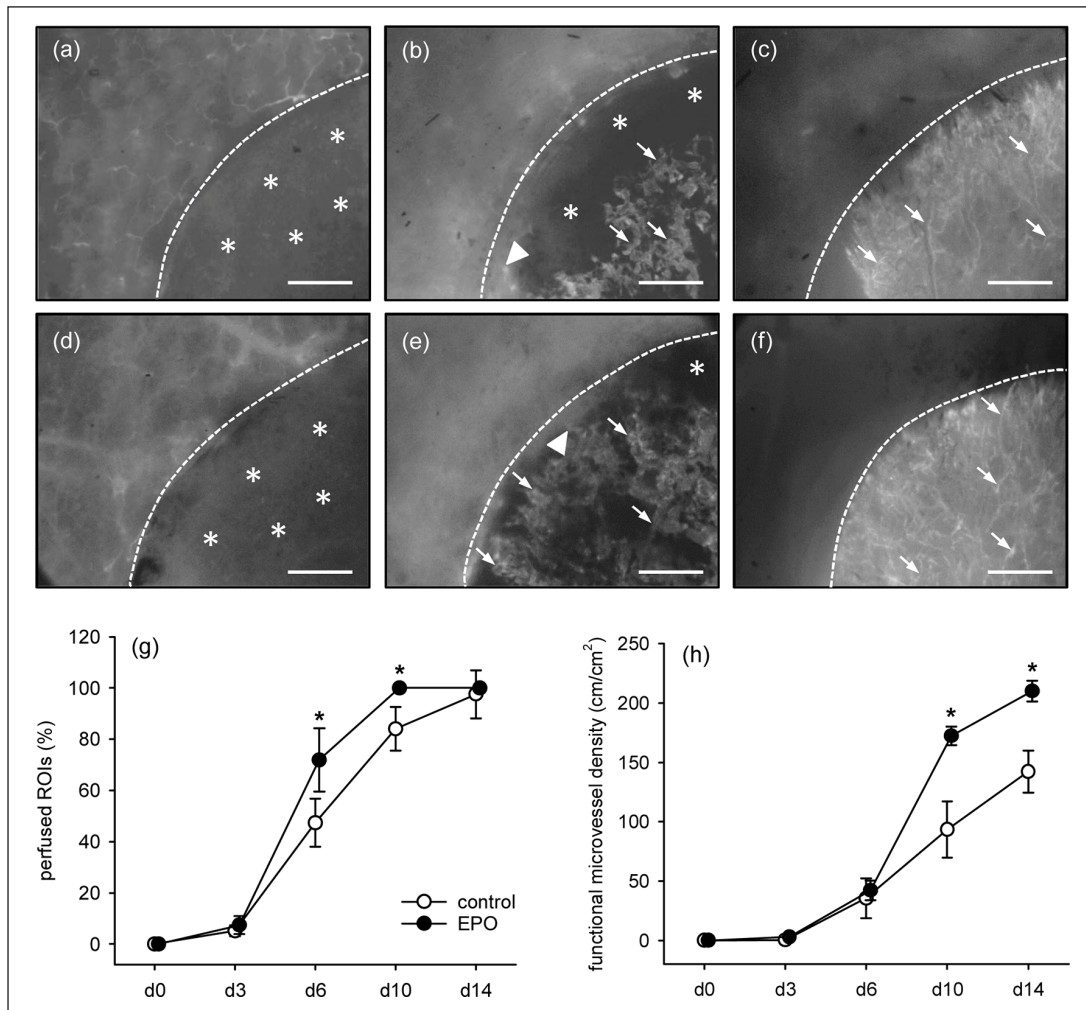
Figure 3. Blood perfusion of implanted MVF-seeded CGAG matrices: (a–f) intravital fluorescence microscopy (blue light epi-illumination, 5% FITC-labeled dextran 150.000 i.v.) of MVF-seeded CGAG matrices on day 0 (a, d), 6 (b, e), and 14 (c, f) after implantation into full-thickness skin defects within dorsal skinfold chambers of vehicle- (a–c) and EPO-treated (d–f) C57BL/6 mice. Broken lines = matrix borders, arrows = perfused microvessels, arrowheads = interconnections of seeded MVF with microvessels of the surrounding host tissue, asterisks = non-perfused matrix areas. Scale bars: 500 μm. (g, h) perfused ROIs (g, %) and functional microvessel density (h, cm/cm²) of MVF-seeded matrices in vehicle- (control; white circles; $n = 8$) and EPO-treated (black circles; $n = 8$) C57BL/6 mice directly (d0) as well as 3, 6, 10, and 14 days after implantation, as assessed by intravital fluorescence microscopy and computer-assisted image analysis. Means ± SEM. *$p < 0.05$ versus control.

Table 1. Diameter (μm), centerline RBC velocity (μm/s), and wall shear rate (s^{-1}) of individual microvessels within MVF-seeded matrices in vehicle- (control; $n = 8$) and EPO-treated ($n = 8$) C57BL/6 mice directly (d0) as well as 3, 6, 10, and 14 days after implantation, as assessed by intravital fluorescence microscopy and computer-assisted image analysis.

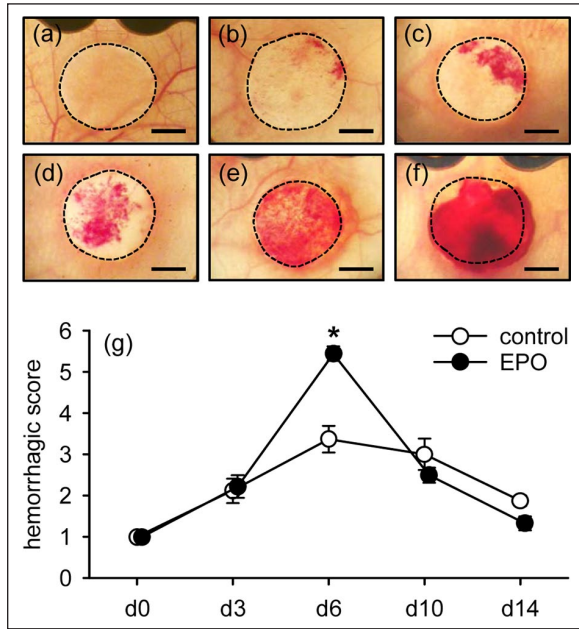|	0 d	3 d	6 d	10 d	14 d
Diameter (μm):					
Control	–	55.7 ± 3.5	34.2 ± 3.0	21.8 ± 2.0	17.0 ± 1.8
EPO	–	54.2 ± 15.0	31.0 ± 1.9	14.4 ± 0.9*	11.3 ± 1.1*
Centerline RBC velocity (μm/s):					
Control	–	22.8 ± 14.0	152.2 ± 30.3	271.8 ± 46.6	273.4 ± 34.6
EPO	35.6 ± 16.4	153.6 ± 40.3	256.9 ± 26.3	300.7 ± 33.9	
Wall shear rate (s^{-1}):					
Control	–	3.6 ± 2.4	36.7 ± 6.3	107.4 ± 20.2	136.6 ± 20.4
EPO	–	7.0 ± 4.0	42.6 ± 11.6	150.6 ± 23.5	232.7 ± 33.9

Mean ± SEM.
*$p < 0.05$ versus control.

Figure 4. Implant-induced bleeding: (a–f) representative trans-illumination stereomicroscopic images according to the semi-quantitative hemorrhagic score, that is, 1: no bleeding (a), 2: 1%–25% (b), 3: 26%–50% (c), 4: 51%–75% (d), 5: 76%–100% (e), 6: bleeding exceeding implant surface (f). Scale bars: 1.4 mm, and (g) hemorrhagic score of MVF-seeded matrices in vehicle- (control; white circles; $n = 8$) and EPO-treated (black circles; $n = 8$) C57BL/6 mice directly (d0) as well as 3, 6, 10, and 14 days after implantation, as assessed by stereomicroscopy. Means ± SEM. *$p < 0.05$ versus control.

showed a comparable infiltration of a dense granulation tissue into matrices seeded with EPO-treated (4047 ± 466 cells/mm²) and vehicle-treated (3748 ± 363 cells/mm²) MVF (Figure 5(a) and (b)). Further quantitative analyses of Sirius red-stained sections revealed a comparable amount of mature collagen fibers within the implanted matrices of both groups (Figure 5(c)–(f)).

Although not proven to be significant, matrices seeded with EPO-treated MVF exhibited a higher density of CD31^{+} microvessels when compared to controls (Figure 6(a)–(c)). Of interest, additional CD31/GFP co-stainings showed a tendency toward a lower fraction of GFP[+] microvessels originating from the seeded GFP[+] MVF within the EPO group (Figure 6(d)–(g)).

Implant epithelialization

Finally, repetitive epi-illumination stereomicroscopy revealed an accelerated epithelialization of matrices seeded with EPO-treated MVF, as indicated by a significantly larger epithelialized area when compared to controls on day 10 after implantation (Figure 7(a)–(g)).

Discussion

MVF represent highly angiogenic vascularization units, which are widely used to study basic mechanisms of microvascular network formation.[30–34] Moreover, they are able to improve the vascularization of different tissue
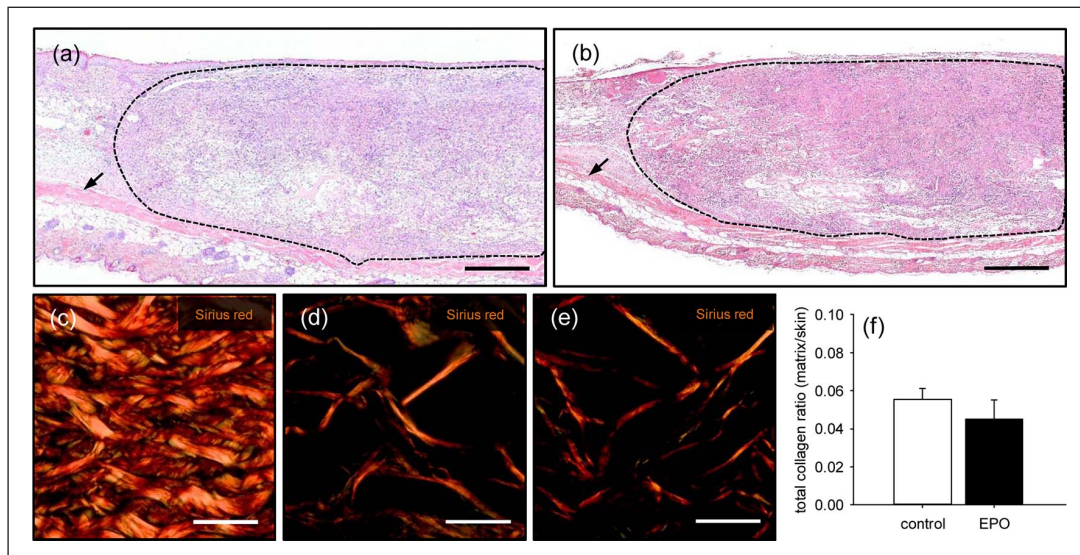

Figure 5. Incorporation of implanted MVF-seeded CGAG matrices: (a, b) HE-stained sections of MVF-seeded CGAG matrices on day 14 after implantation into full-thickness skin defects within the dorsal skinfold chamber of a vehicle- (a) and an EPO-treated (b) C57BL/6 mouse (broken lines = matrix borders, arrows = panniculus carnosus muscle). Scale bars: 400 μm. (c–e) polarized light microscopy of Sirius red-stained sections of normal skin (c) as well as MVF-seeded CGAG matrices on day 14 after implantation into full-thickness skin defects within the dorsal skinfold chamber of a vehicle- (d) and an EPO-treated (e) C57BL/6 mouse. Scale bars: 35 μm, and (f) total collagen ratio (matrix/skin) of MVF-seeded matrices in vehicle- (control; white bar; $n = 8$) and EPO-treated (black bar; $n = 8$) C57BL/6 mice on day 14 after implantation, as assessed by polarized light microscopy of Sirius red-stained sections. Means ± SEM. *$p < 0.05$ versus control.
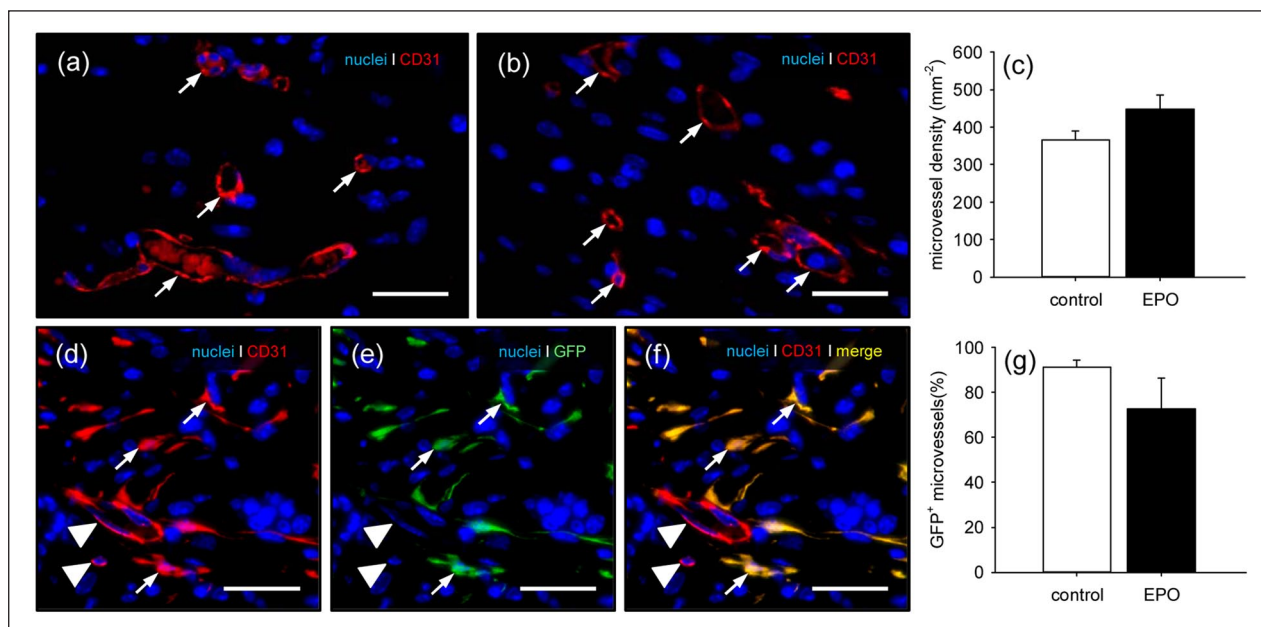
Figure 6. Vascularization of implanted MVF-seeded CGAG matrices: (a, b) immunohistochemical detection of CD31^{+} microvessels (arrows) in MVF-seeded CGAG matrices on day 14 after implantation into full-thickness skin defects within the dorsal skinfold chamber of a vehicle- (a) and an EPO-treated (b) C57BL/6 mouse. Scale bars: 30 μm, (c) microvessel density (mm^{−2}) of MVF-seeded matrices in vehicle- (control; white bar; $n = 8$) and EPO-treated (black bar; $n = 8$) C57BL/6 mice on day 14 after implantation, as assessed by immunohistochemical analysis. Means $\pm$ SEM, (d–f) immunohistochemical detection of CD31^{+}/GFP^{+} microvessels (arrows) and CD31^{+}/GFP^{−} microvessels (arrowheads) in a MVF-seeded CGAG matrix on day 14 after implantation into a full-thickness skin defect within the dorsal skinfold chamber of an EPO-treated C57BL/6 mouse. Scale bars: 30 μm, and (g) GFP[+] microvessels (%) in MVF-seeded matrices of vehicle- (control; white bar; $n = 8$) and EPO-treated (black bar; $n = 8$) C57BL/6 mice on day 14 after implantation, as assessed by immunohistochemical analysis. Means $\pm$ SEM.

types.[35–39] Of interest, recent studies have shown that the vascularization capacity of MVF can be further enhanced by exposure to growth factors.[11,40] In fact, we found that a 24-h precultivation in medium supplemented with EPO improves the viability of MVF and promotes their reassembly into new microvascular networks after seeding onto CGAG matrices and in vivo implantation.[11] In the present follow-up study, we demonstrate that a systemically applied low dose of EPO induces similar effects without the necessity of a time-consuming pre-cultivation phase of MVF.

Of note, the herein used protocol for EPO treatment was chosen according to Rezaeian et al.[18], who reported that the application of the glycoprotein shows maximum beneficial effects on blood perfusion and angiogenesis of critically perfused flap tissue when administered in an overlapping regime, that is, before and after the surgical intervention. Accordingly, we also exposed MVF to systemic EPO doses before their isolation from donor fat samples as well as after their transfer into tissue defects of recipient mice. For this purpose, we used repetitive low doses of 500 IU/kg EPO, which have been proven to neither affect hematocrit nor hemoglobin levels even when administered for 20 days.[18] Considering the short half-life of EPO,[41] this repetitive EPO treatment may have ideally

supported the reassembly of MVF into new microvascular networks during the first days after matrix implantation.

In a first set of experiments, we isolated MVF from the epididymal fat tissue of EPO- and vehicle-treated donor mice to analyze their proliferation and viability. We did not detect a stimulatory effect of EPO on the proliferation of endothelial cells. In contrast, EPO-treated MVF exhibited a lower fraction of apoptotic endothelial cells when compared to vehicle-treated controls. The latter finding is in line with the results of various other studies demonstrating anti-apoptotic effects of EPO. For instance, the glycoprotein inhibits apoptosis of rat microglial cells in vitro[42] and suppresses neuronal apoptosis in a rodent model of closed head injury.[22] Of particular relevance for the present study, EPO has been further shown to reduce apoptotic cell death of adipose tissue[43] as well as endothelial progenitor cells[44] and mature endothelial cells.[45]

We investigated the effects of systemic low-dose EPO treatment on MVF-seeded CGAG matrices in the dorsal skinfold chamber model. In combination with intravital fluorescence microscopy, this approach not only allows the repetitive analysis of microvascular network formation within implanted matrices, but also the assessment of the functionality of individual microvessels, as indicated by fluorescently labeled blood perfusion.[29] We could
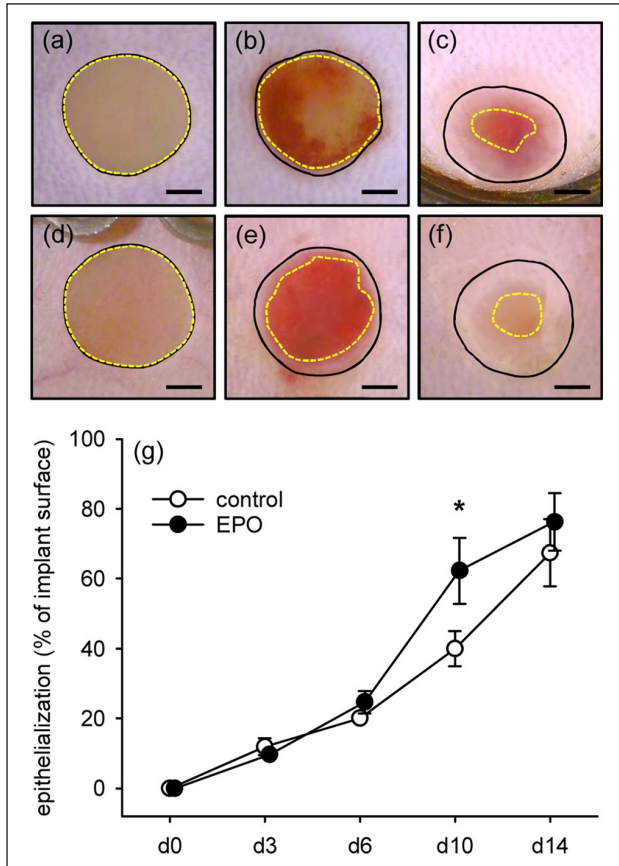
Figure 7. Epithelialization of implanted MVF-seeded CGAG matrices (a–f) stereomicroscopic images of CGAG matrices on day 0 (a, d), 6 (b, e), and 14 (c, f) after implantation into full-thickness skin defects within dorsal skinfold chambers of vehicle- (a–c) and EPO-treated (d–f) C57BL/6 mice. Closed lines = matrix borders, broken lines = non-epithelialized matrix areas. Scale bars: 1 mm, and (g) epithelialization (%) of MVF-seeded matrices in vehicle- (control; white circles; $n = 8$) and EPO-treated (black circles; $n = 8$) C57BL/6 mice directly (d0) as well as 3, 6, 10, and 14 days after implantation, as assessed by stereomicroscopy.
Means ± SEM. *$p < 0.05$ versus vehicle.

demonstrate that MVF-seeded CGAG matrices within EPO-treated mice reveal both significantly more perfused ROIs on days 6 and 10 as well as a higher functional microvessel density on days 10 and 14 when compared to matrices in vehicle-treated animals. This may be due to the fact that EPO is a potent angiogenic factor,[46,47] which activates different angiogenic signal transduction pathways, such as JAK2/STAT5 and AMPK-KLF2.[48,49] In addition, the maturation of microvessels within the CGAG matrices of EPO-treated mice was more pronounced, as indicated by significantly smaller vessel diameters on both days 10 and 14 after implantation. This accelerated maturation may be explained by an EPO/EPOR-mediated enhanced proliferation of smooth muscle cells,[50] which are responsible for the stabilization of blood vessels.

In line with our intravital fluorescence microscopic findings, we further detected a significantly elevated hemorrhage formation within EPO-treated animals when compared to vehicle-treated controls on day 6. At this early time point, the matrices of the EPO group already exhibited an improved perfusion. On the other hand, the newly developing microvascular networks may have still contained many immature microvessels with an increased permeability causing elevated bleeding. However, due to the fact that the semiquantitative score of hemorrhage formation within EPO-treated mice rapidly returned back to the baseline level of day 0, this observation has to be interpreted as an EPO-induced temporary vascularization boost.

At the end of the 14-day observation period, we finally analyzed the implanted MVF-seeded CGAG matrices by means of histology and immunohistochemistry. These analyses revealed that neither the cellular infiltration into the implants nor their collagen content markedly differed between the two groups. However, the matrices in EPO-treated mice exhibited a tendency toward a higher microvessel density when compared to those in vehicle-treated controls. In addition, they revealed a reduced fraction of $CD31^+/GFP^+$ microvessels. These results indicate that EPO may have particularly stimulated the early angiogenic ingrowth of $CD31^+/GFP^-$ microvessels from the surrounding host tissue into the matrices without improving the endothelial proliferating activity of the $CD31^+/GFP^+$ MVF.

Finally, our stereomicroscopic analysis of the implants showed a significantly improved epithelialization of CGAG matrices in EPO-treated animals when compared to vehicle-treated controls on day 10. This positive effect of EPO on skin repair has previously been described in other wound healing studies and may be explained by the stimulatory effect of this glycoprotein on the proliferating and migratory activity of fibroblasts and keratinocytes.[28,51]

Conclusion

The present study demonstrates that systemic low-dose EPO treatment improves the vascularization capacity of MVF. This type of treatment enhances their viability and promotes the vascularization and epithelialization of MVF-seeded matrices after implantation. Given the fact that EPO is already approved for the use in patients, the herein applied MVF-based vascularization approach may be easily combined with EPO treatment in future clinical practice.

Declaration of conflicting interests

The author(s) declared no potential conflicts of interest with respect to the research, authorship, and/or publication of this article.

Ethical approval

All animal experiments were approved by the local governmental animal protection committee (permit number: 39/2018) and conducted in accordance with the European legislation on the protection of animals (Directive 2010/63/EU) and the NIH guidelines on the care and use of laboratory animals (NIH publication #85-23 Rev. 1985).

ORCID iDs

Thomas Später   https://orcid.org/0000-0002-1008-6376

Matthias W Laschke   https://orcid.org/0000-0002-7847-8456

Availability of data and materials

All the data can be obtained in this manuscript.

References

1. MacNeil S. Progress and opportunities for tissue-engineered skin. *Nature* 2007; 445: 874–880.
2. Kneilling M, Breuninger H, Schippert W, et al. A modified, improved, easy and fast technique for split-thickness skin grafting. *Br J Dermatol* 2011; 165: 581–584.
3. Halim AS, Khoo TL and Mohd Yussof SJ. Biologic and synthetic skin substitutes: an overview. *Indian J Plast Surg* 2010; 43: S23–S28.
4. Zhong SP, Zhang YZ and Lim CT. Tissue scaffolds for skin wound healing and dermal reconstruction. *Wiley Interdiscip Rev Nanomed Nanobiotechnol* 2010; 2: 510–525.
5. Trottier V, Marceau-Fortier G, Germain L, et al. IFATS collection: using human adipose-derived stem/stromal cells for the production of new skin substitutes. *Stem Cells* 2008; 26: 2713–2723.
6. Awad HA, Butler DL, Harris MT, et al. In vitro characterization of mesenchymal stem cell-seeded collagen scaffolds for tendon repair: effects of initial seeding density on contraction kinetics. *J Biomed Mater Res* 2000; 51: 233–240.
7. Biedermann T, Klar AS, Böttcher-Haberzeth S, et al. Tissue-engineered dermo-epidermal skin analogs exhibit de novo formation of a near natural neurovascular link 10 weeks after transplantation. *Pediatr Surg Int* 2014; 30: 165–172.
8. Frueh FS, Später T, Lindenblatt N, et al. Adipose tissue-derived microvascular fragments improve vascularization, lymphangiogenesis, and integration of dermal skin substitutes. *J Invest Dermatol* 2017; 137: 217–227.
9. Frueh FS, Später T, Scheuer C, et al. Isolation of murine adipose tissue-derived microvascular fragments as vascularization units for tissue engineering. *J Vis Exp* 2017; 122: 55721.
10. Später T, Körbel C, Frueh FS, et al. Seeding density is a crucial determinant for the in vivo vascularisation capacity of adipose tissue-derived microvascular fragments. *Eur Cell Mater* 2017; 34: 55–69.
11. Karschnia P, Scheuer C, Heß A, et al. Erythropoietin promotes network formation of transplanted adipose tissue-derived microvascular fragments. *Eur Cell Mater* 2018; 35: 268–280.
12. Eschbach JW, Kelly MR, Haley NR, et al. Treatment of the anemia of progressive renal failure with recombinant human erythropoietin. *N Engl J Med* 1989; 321: 158–163.
13. Ruedin P, Pechère Bertschi A, Chapuis B, et al. Safety and efficacy of recombinant human erythropoietin treatment of anaemia associated with multiple myeloma in haemodialysed patients. *Nephrol Dial Transplant* 1993; 8: 315–318.
14. Adam Z, Krahulová M, Spelda S, et al. Therapy of anemia in patients with multiple myeloma. *Acta Med Austriaca* 1995; 22: 59–64.
15. Chavin SI. Erythropoietin therapy for anemia. *J Am Geriatr Soc* 1995; 43: 314–315.
16. Hardee ME, Arcasoy MO, Blackwell KL, et al. Erythropoietin biology in cancer. *Clin Cancer Res* 2006; 12: 332–329.
17. Singh AK, Szczech L, Tang KL, et al. Correction of anemia with epoetin alfa in chronic kidney disease. *N Engl J Med* 2006; 355: 2085–2098.
18. Rezaeian F, Wettstein R, Amon M, et al. Erythropoietin protects critically perfused flap tissue. *Ann Surg* 2008; 248: 919–929.
19. Tilbrook PA and Klinken SP. The erythropoietin receptor. *Int J Biochem Cell Biol* 1999; 31: 1001–1005.
20. Mulcahy L. The erythropoietin receptor. *Semin Oncol* 2001; 28: 19–23.
21. Haroon ZA, Amin K, Jiang X, et al. A novel role for erythropoietin during fibrin-induced wound-healing response. *Am J Pathol* 2003; 163: 993–1000.
22. Yatsiv I, Grigoriadis N, Simeonidou C, et al. Erythropoietin is neuroprotective, improves functional recovery, and reduces neuronal apoptosis and inflammation in a rodent model of experimental closed head injury. *FASEB J* 2005; 19: 1701–1703.
23. Calvillo L, Latini R, Kajstura J, et al. Recombinant human erythropoietin protects the myocardium from ischemia-reperfusion injury and promotes beneficial remodeling. *Proc Natl Acad Sci U S A* 2003; 100: 4802–4806.
24. Ribatti D, Presta M, Vacca A, et al. Human erythropoietin induces a pro-angiogenic phenotype in cultured endothelial cells and stimulates neovascularization in vivo. *Blood* 1999; 93: 2627–2636.
25. Crivellato E, Nico B, Vacca A, et al. Recombinant human erythropoietin induces intussusceptive microvascular growth in vivo. *Leukemia* 2004; 18: 331–336.
26. Kertesz N, Wu J, Chen TH, et al. The role of erythropoietin in regulating angiogenesis. *Dev Biol* 2004; 276: 101–110.
27. Hoying JB, Boswell CA and Williams SK. Angiogenic potential of microvessel fragments established in three-dimensional collagen gels. *In Vitro Cell Dev Biol Anim* 1996; 32: 409–419.
28. Sorg H, Krueger C, Schulz T, et al. Effects of erythropoietin in skin wound healing are dose related. *FASEB J* 2009; 23: 3049–3058.
29. Laschke MW and Menger MD. The dorsal skinfold chamber: a versatile tool for preclinical research in tissue engineering and regenerative medicine. *Eur Cell Mater* 2016; 32: 202–215.
30. Kirkpatrick ND, Andreou S, Hoying JB, et al. Live imaging of collagen remodeling during angiogenesis. *Am J Physiol Heart Circ Physiol* 2007; 292: H3198–H3206.

31. Edgar LT, Underwood CJ, Guilkey JE, et al. Extracellular matrix density regulates the rate of neovessel growth and branching in sprouting angiogenesis. *PLoS One* 2014; 9: e85178.

32. Utzinger U, Baggett B, Weiss JA, et al. Large-scale time series microscopy of neovessel growth during angiogenesis. *Angiogenesis* 2015; 18: 219–232.

33. Später T, Frueh FS, Nickels RM, et al. Prevascularization of collagen-glycosaminoglycan scaffolds: stromal vascular fraction versus adipose tissue-derived microvascular fragments. *J Biol Eng* 2018; 12: 24.

34. Später T, Menger MM, Nickels RM, et al. Macrophages promote network formation and maturation of transplanted adipose tissue-derived microvascular fragments. *J Tissue Eng* 2020; 11: 2041731420911816.

35. Nakano M, Nakajima Y, Kudo S, et al. Effect of autotransplantation of microvessel fragments on experimental random-pattern flaps in the rat. *Eur Surg Res* 1998; 30: 149–160.

36. Nakano M, Nakajima Y, Kudo S, et al. Successful autotransplantation of microvessel fragments into the rat heart. *Eur Surg Res* 1999; 31: 240–248.

37. Shepherd BR, Hoying JB and Williams SK. Microvascular transplantation after acute myocardial infarction. *Tissue Eng* 2007; 13: 2871–2879.

38. Hiscox AM, Stone AL, Limesand S, et al. An islet-stabilizing implant constructed using a preformed vasculature. *Tissue Eng Part A* 2008; 14: 433–440.

39. Pilia M, McDaniel JS, Guda T, et al. Transplantation and perfusion of microvascular fragments in a rodent model of volumetric muscle loss injury. *Eur Cell Mater* 2014; 28: 11–23.

40. Laschke MW, Kontaxi E, Scheuer C, et al. Insulin-like growth factor 1 stimulates the angiogenic activity of adipose tissue-derived microvascular fragments. *J Tissue Eng* 2019; 10: 2041731419879837.

41. Vairano M, Dello Russo C, Pozzoli G, et al. Erythropoietin exerts anti-apoptotic effects on rat microglial cells in vitro. *Eur J Neurosci* 2002; 16: 584–592.

42. Lee DE, Son W, Ha BJ, et al. The prolonged half-lives of new erythropoietin derivatives via peptide addition. *Biochem Biophys Res Commun* 2006; 339: 380–385.

43. Hamed S, Egozi D, Kruchevsky D, et al. Erythropoietin improves the survival of fat tissue after its transplantation in nude mice. *PLoS One* 2010; 5: e13986.

44. Cheng Y, Hu R, Lv L, et al. Erythropoietin improves the efficiency of endothelial progenitor cell therapy after myocardial infarction in mice: effects on transplanted cell survival and autologous endothelial progenitor cell mobilization. *J Surg Res* 2012; 176: e47–e55.

45. Gammella E, Leuenberger C, Gassmann M, et al. Evidence of synergistic/additive effects of sildenafil and erythropoietin in enhancing survival and migration of hypoxic endothelial cells. *Am J Physiol Lung Cell Mol Physiol* 2013; 304: L230–L239.

46. Galeano M, Altavilla D, Cucinotta D, et al. Recombinant human erythropoietin stimulates angiogenesis and wound healing in the genetically diabetic mouse. *Diabetes* 2004; 53: 2509–2517.

47. Li Y, Lu Z, Keogh CL, et al. Erythropoietin-induced neurovascular protection, angiogenesis, and cerebral blood flow restoration after focal ischemia in mice. *J Cereb Blood Flow Metab* 2007; 27: 1043–1054.

48. Ribatti D, Vacca A, Roccaro AM, et al. Erythropoietin as an angiogenic factor. *Eur J Clin Invest* 2003; 33: 891–896.

49. Wang D, Song Y, Zhang J, et al. AMPK-KLF2 signaling pathway mediates the proangiogenic effect of erythropoietin in endothelial colony-forming cells. *Am J Physiol Cell Physiol* 2017; 313: C674–C685.

50. Ammarguellat F, Gogusev J and Drüeke TB. Direct effect of erythropoietin on rat vascular smooth-muscle cell via a putative erythropoietin receptor. *Nephrol Dial Transplant* 1996; 11: 687–692.

51. Galeano M, Altavilla D, Bitto A, et al. Recombinant human erythropoietin improves angiogenesis and wound healing in experimental burn wounds. *Crit Care Med* 2006; 34: 1139–1146.